Control Law Synthesis for an Airplane with Relaxed Static Stability

J.D. Blight,* D. Gangsaas,† and T.M. Richardson‡
Boeing Military Airplane Company, Seattle, Washington

The synthesis of a command and stability augmentation control law for a transport airplane is presented. To improve fuel efficiency, the airplane has a relatively small horizontal tail surface and therfore has unsatisfactory inherent longitudinal stability. Over a wide range of center-of-gravity locations and the full flight envelope, the control law furnishes 1) task tailored column force gradients; 2) excellent dynamic responses for normal acceleration, pitch rate, and speed; and 3) better than $\zeta = 0.5$ damping for the phugoid and short period modes. The control law is based on linear quadratic Gaussian synthesis at a single operating point. The gains are scheduled as functions of dynamic pressure and airplane flap position. The control is the elevator command and the sensors are column force, normal acceleration, pitch rate, airspeed, longitudinal acceleration, and vertical speed.

Nomenclature

c.g. = center of gravity
$C_{m\alpha}$ = variation of pitching moment coefficient with angle of attack
$E[\cdot]$ = expected value
F_c = column force, lb
$\dot{h}$ = vertical speed, ft/s
I_{nzu} = cost function variable, g
J = cost function
K_{ct} = V_{CAS}/V_T ratio, knots/(ft/s)
K_F = feedforward gain, g/lb
K_I = internal cost function parameter, s^{-1}
K_n = feedback gain parameter, g/knot
K_u = cost function parameter, g/knot
LQ = linear quadratic
LQG = linear quadratic Gaussian
LQR = linear quadratic regulator
MAC = mean aerodynamic chord
n_z = normal acceleration, g
n_{zu} = linear combination of normal acceleration and airspeed, g
q = pitch rate, deg/s
q_c = dynamic pressure, lb/ft^2
Q_u, Q_c = cost function output weighting parameters
rms = root mean square
s_n = wind shear noise, ft/s^3
u = inertial speed, ft/s
u_g = horizontal gust velocity, ft/s
u_{mw} = mean horizontal wind speed, ft/s
$u_{mr}, \dot{u}_{mw}$ = mean wind rate, ft/s^2
V_{CAS} = calibrated airspeed, knots
V_m = mean airspeed, knots or ft/s
V_T = true airspeed, ft/s
w_g = vertical gust velocity, ft/s
w_{g1} = intermediate vertical gust state
y_c, y_u = cost function criteria
α = angle of attack, deg
δ_e = elevator angle, deg
δ_{ec} = elevator servo command, deg
δ_f = flap position
δ_{servo} = elevator servo angle, deg
θ = pitch angle, deg
σ = rms intensity
$(\ )_n$ = noise quantity

Submitted April 19, 1986. Revision received June 2, 1986.

*Principal Engineer, Flight Controls Technology Research.
†Unit Chief, Flight Controls Technology Research. Associate Fellow AIAA.
‡Supervisor, Flight Controls Technology Research.

Introduction

TRADITIONALLY, transport airplanes have been designed to have a certain level of inherent longitudinal stability. This and other control requirements dictate the size of the horizontal tail and restrict the permissible most-aft location of the center of gravity (c.g.). The efficiency of these airplanes can be improved by decreasing the horizontal tail size and moving the c.g. aft. The corresponding reductions in weight and trim drag from the decreased tail size and trim load on the tail can yield a significant reduction in fuel consumption.[1]

However, these airplanes will have unsatisfactory longitudinal stability and control characteristics within part of their c.g. and flight envelopes. Figure 1 shows typical time responses to a step elevator input for such an airplane. Figure 2 shows the corresponding long-term speed response of the airplane. The airplane response is unstable with the aft c.g. location. A command and stability augmentation system is required to provide satisfactory airplane stability and control characteristics. The control law development for such a system is described in this paper.

Requirements and Objectives

The following were the main design requirements and objectives:

1) Satisfy flying qualities requirements of Refs. 2 and 3.

2) Furnish constant or task-tailored pilot column force gradients with respect to commanded normal acceleration and airspeed changes across the c.g. range and flight envelope.

3) Provide short-period and phugoid mode damping ratios greater than 0.5.

4) Turbulence and wind shear response must be as good as or better than current airplanes.

5) Satisfy ±10 dB gain margin and ±45 deg phase margin within the control bandwidth.

6) The loop gain crossover frequency must not exceed 3 rad/s and the high-frequency loop gain must be below −10 dB at 10 rad/s with a minimum of −40 dB/decade slope beyond 10 rad/s to avoid destabilizing unmodeled structural modes at these higher frequencies.

7) Gain scheduling must be functions of easily measured parameters.

Open-Loop Airplane Characteristics

The open-loop airplane stability and response characteristics were determined for several flight conditions. The latter are defined in Table 1. Figures 1-4 show the airplane response to an elevator input. In Table 2, the eigenvalues are listed for the four flight conditions. There are significant variations in the airplane response characteristics between the different flight conditions and due to changes in the c.g. location. Except for the landing conditions, the airplane is unstable with the c.g. at the aft location.

Control Law Synthesis

The airplane and wind dynamics were described by linear time invariant state space models for the four flight conditions. The control law synthesis was performed based on the cruise flight condition with the center of gravity at 50% MAC. Analysis was performed and the gain schedules were developed based on all flight conditions described in Table 1. The synthesis was accomplished using linear quadratic Gaussian (LQG) synthesis with loop shaping.[4-9]

Figure 5 shows the model used in the linear quadratic regulator (LQR) synthesis. The disturbance model consists of longitudinal and vertical Dryden turbulence models[10] and a horizontal wind shear model. In addition to the airplane, turbulence and wind shear models, an ideal column force command model defining desired transient and steady-state response characteristics, and a model of a high-pass filtered output of the control input were included to adjust the control loop gain rolloff characteristics at high frequencies. The total synthesis model is given in the Appendix.

The gains were calculated to minimize the cost function

$$J = (\tfrac{1}{2})E[Q_u y_u^2 + Q_c y_c^2 + \delta_{ec}^2] \quad (1)$$

This cost function was constructed to reflect the design requirements for: 1) transient and steady-state command response characteristics; 2) good turbulence and wind shear response; 3) insensitivity to model errors and parameter variations within the control bandwidth; 4) robustness with respect to unmodeled dynamics outside the control bandwidth; 5) well-behaved crossover characteristics; and 6) good damping of all modes.

The control input was the elevator servo command δ_{ec}. There were two output criterion variables y_u and y_c. The

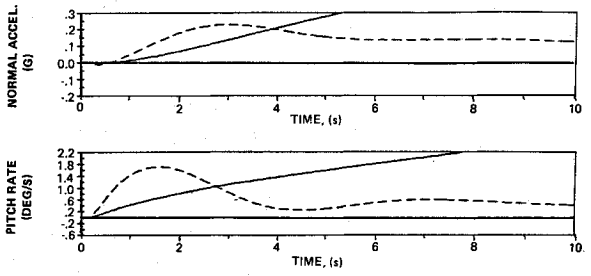

Fig. 1 Short-period response of open-loop airplane at V_{min} flight condition.

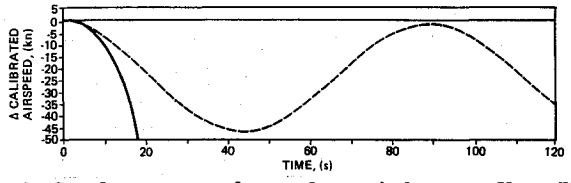

Fig. 2 Speed response of open-loop airplane at V_{min} flight condition.

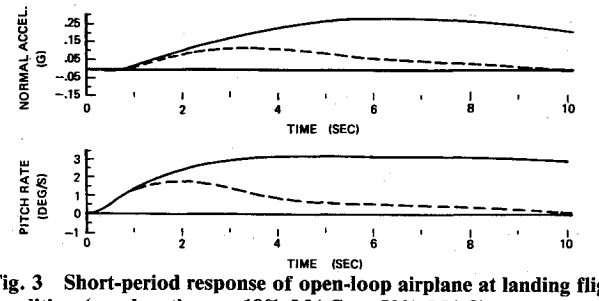

Fig. 3 Short-period response of open-loop airplane at landing flight condition (c.g. location: ---18% MAC, —50% MAC).

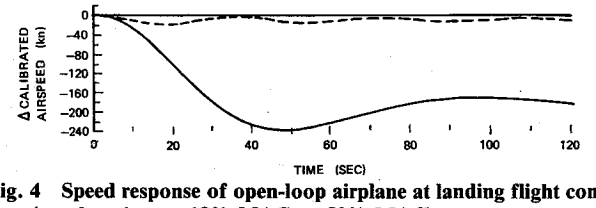

Fig. 4 Speed response of open-loop airplane at landing flight condition (c.g. location: ---18% MAC, —50% MAC).

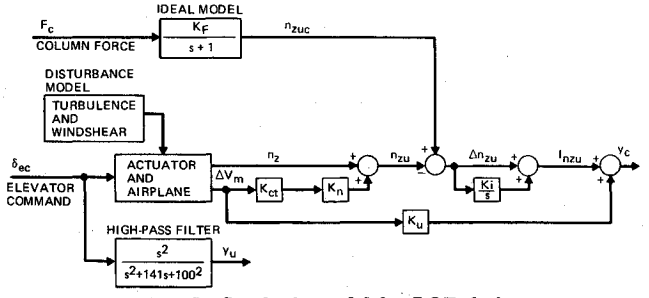

Fig. 5 Synthesis model for LQR design.

Table 1 Flight conditions

	Flight conditions			
Condition	Cruise	V_{min}	Landing	V_{FC}/M_{FC}
Mach	0.80	0.57	0.19	0.87
V_{CAS}, knot	272	189	125	366
V_T, ft/s	778	555	214	882
Dynamic pressure, lb/ft^2	261	123	53	490
Altitude, ft	35,000	35,000	1,000	25,500
Flight path angle, deg	0	0	−3	−1
Flaps	0	0	30	0
Landing gear	Up	Up	Down	Up
Weight, lb	184,000	184,000	184,000	184,000

criterion y_u was included to adjust the high-frequency gain attenuation in the control loop. The criterion y_c represents the regulated output. It comprises a combination of the errors in mean airspeed ΔV_m and normal acceleration Δn_z with integral control added, as shown in Fig. 5.

For a stable airplane in wings level flight, a small column force input producing an elevator deflection will result in an initial incremental normal acceleration that returns to zero and a slower speed response that settles to a new steady-state value. The sensitivities between the column force input and 1) the normal acceleration response (lb/g) with the airspeed unchanged and 2) the long-term airspeed response (lb/knot) with the incremental normal acceleration unchanged are key parameters in determining the flying qualities of an airplane. They must lie within certain bounds.[2]

Referring to Fig. 5, it can be seen that with the control law structure defined in the figure, the feedforward gain K_F (g/lb) and speed feedback gain K_n (g/knot) completely define these parameters for a stable closed-loop system due to the presence of the feedback integrator. Based on the guidelines in Ref. 2 and piloted simulations, column force gradients of 30 lb/g and $-\frac{1}{4}$ lb/knot were selected for this application. The corresponding values for K_F and K_n were 1/30 g/lb and $-1/120$ g/knot, respectively. For other applications, these parameters can be changed to reflect the unique flying qualities requirements for specific pilot tasks and flight phases. The remaining gains K_I and K_u and the location of the sensor measuring normal acceleration n_z were adjusted to obtain good frequency domain loop shapes between the control input δ_{ec} and the regulated outputs y_c.

Figure 6 shows the frequency response between the elevator and the normal acceleration measured at a forward location. As expected for a small-perturbation longitudinal airplane model, there is a zero near the origin.[11] This confirms the earlier statement that nonzero normal acceleration cannot be maintained in the steady-state using the elevator. There is also a pair of lightly damped zeros at a frequency of approximately 3 rad/s. This would result in poor damping of the short-period mode as the loop gain is increased. A zero locus was calculated as a function of the longitudinal position of the normal acceleration sensor. At a location just forward of the center of gravity, the zeros are located on the real axis at -16 and 60 rad/s outside the expected control loop bandwidth. The corresponding frequency response is shown in Fig. 7. This loop shape will ensure good closed-loop characteristics of the short-period mode.

Figure 8 shows the frequency response between the elevator input and the airspeed output. As expected for a linear longitudinal airplane model, there is significant gain at low frequency.[11] This confirms that speed can be controlled in the steady-state from the elevator. Combining speed feedback with normal acceleration feedback provides the required nonzero gain at zero frequency. Figure 9 shows the frequency response between the elevator and the output n_{zu}. The latter is a linear combination of mean airspeed error and normal acceleration defined as

$$n_{zu} = n_z + K_n \Delta V_m \tag{2}$$

K_n was selected together with K_F (see Fig. 5) to provide the

Table 2 Engenvalues of the open-loop airplane

	Flight condition			
C.g. location	Cruise	V_{min}	V_{FC}/M_{FC}	Landing
18% MAC	$-0.0064 \pm j0.060$ $-.865 \pm j.190$	$-0.0084 \pm j.694$ $-.433 \pm j1.098$	$-.037 \pm j.089$ $-1.196 \pm j2.13$	$-.013 \pm j.174$ $-.531 \pm j.883$
50% MAC	.012 ($T_2 = 58_s$) $-.0318$ $-.519$ -1.10	.107 ($T_2 = 6.5_s$) $-.0924 \pm j.112$ $-.791$	$.0512 \pm j.251$ ($T_2 = 13.5_s$) -2.09 $-.40$	$-0.28 \pm j.068$ $-.502 \pm j.686$

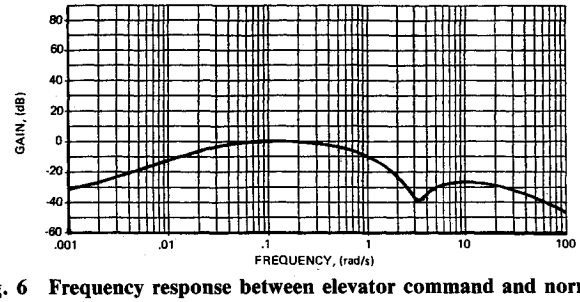

Fig. 6 Frequency response between elevator command and normal acceleration at forward location.

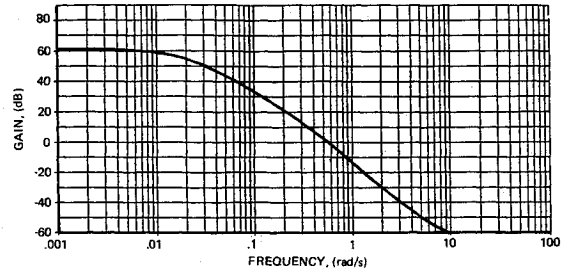

Fig. 8 Frequency response between elevator command and air speed.

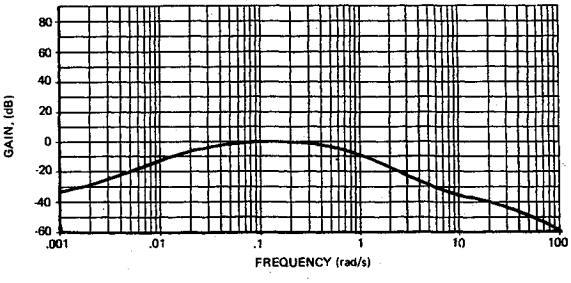

Fig. 7 Frequency response between elevator command and normal acceleration at midlocation.

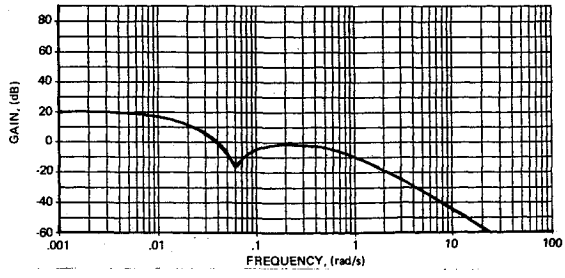

Fig. 9 Frequency response between elevator command and N_{zu}.

desired steady-state column force gradients as described earlier. Mean airspeed error is defined as

$$\Delta V_m = V_m - V_R \tag{3}$$

where V_R is the reference trim airspeed and V_m the mean airspeed. The latter is defined as

$$V_m = u - u_{mw} \tag{4}$$

where u is the inertial speed and u_{mw} the mean horizontal wind speed. In contrast, the true airspeed V_T is defined as

$$V_T = u - u_{mw} - u_g \tag{5}$$

where u_g is the zero mean horizontal gust velocity. The reason mean airspeed is controlled rather than true airspeed is to reduce elevator activity due to horizontal gust inputs. V_m cannot be measured directly and therefore the Kalman filter estimate $\hat{V}_m$ is used for the control law implementation.

In order to meet the requirement for insensitivity to model errors and parameter variations within the control bandwidth, an integral term was added to the output criterion as follows:

$$I_{nzu} = \Delta n_{zu}(1 + K_I/s) \tag{6}$$

where Δn_{zu} is defined in Fig. 5.

A value of $K_I = 1.5$ was selected to ensure good integral control at frequencies at or below 1.5 rad/s. As a result of the zero created at -1.5 rad/s, the closed-loop integral pole will move to this value. The resulting loop transfer function is shown in Fig. 10. There is a pair of lightly damped zeros at a frequency of approximately 0.06 rad/s. These zeros control the damping and frequency of the closed-loop phugoid mode. The location of these zeros can be changed to a more stable location by adjusting the parameter K_n. However, this would change the column force to airspeed gradient away from its desired value. To avoid this, a new airspeed term was added to the output criterion as follows:

$$y_c = I_{nzu} + K_u \Delta V_m \tag{7}$$

For this application, K_u was adjusted to provide damping of $\zeta_{ph} = 0.707$ for the closed-loop phugoid mode. For other applications, the gains K_n and K_u can be adjusted to reflect different requirements for force gradients and phugoid stability characteristics. These can be tailored to specific pilot tasks and flight phases.

Figure 11 shows the frequency response between the elevator command and the regulated output criterion. This loop shape will furnish the desired characteristics in terms of high gain within the control bandwidth, well-behaved crossover, and good damping of the closed-loop modes. The other criterion output, y_u, will ensure additional gain attenuation as required at and beyond a frequency of 10 rad/s.

A full-state control law was synthesized based on the cost function represented by Eq. (1) with the penalty weights Q_u and Q_c as design parameters. These were adjusted to furnish the required elevator loop crossover frequency (between 2 and 3 rad/s) and high-frequency gain attenuation. Figure 12 illustrates that the LQR design meets the requirements for high elevator loop gain at low frequencies, good gain and phase margins, and the required high-frequency gain attenuation. The values for the corresponding penalty weights are given in Table 3. Feedback gains are shown in Table 4.

Having obtained the desired elevator loop shape in the LQR design, a state estimator was synthesized. The objective was to design a feedback compensator that with the available measurements would furnish 1) the same elevator loop shape

Table 3 Full-state design parameters

$R = 1.0$
$Q_c = 7.14$
$Q_u = 714.0$

Table 4 LQR feedback gains

State	Gain
ΔV_m	−0.361
α	1.425
q	1.01
θ	0.244
u_g	−0.024
w_g	−0.068
w_{g1}	−0.0003
$\dot{u}_{mw}$	0.432
$\int \Delta n_{zu}$	−4.437

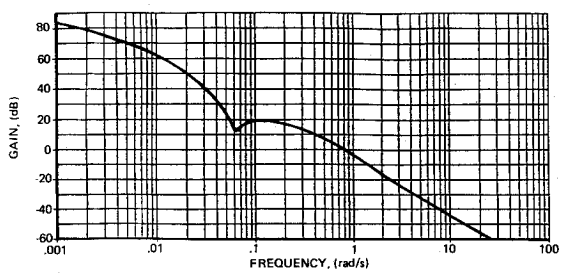

Fig. 10 Frequency response between elevator command and I_{nzu}0.

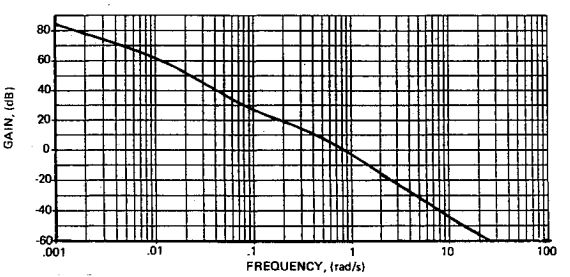

Fig. 11 Frequency response between elevator command and criterion output.

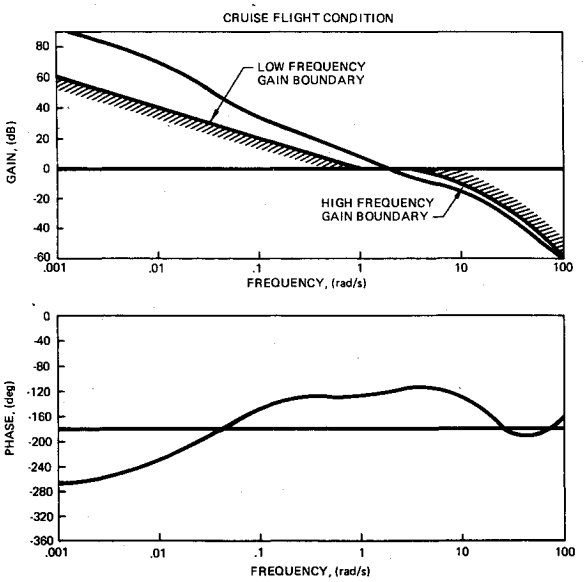

Fig. 12 Elevator open-loop frequency response for LQR full-state feedback design, cruise flight condition.

as the LQR designs and 2) estimates of the horizontal and vertical turbulence velocities, the mean airspeed, and the mean wind speed rate. The former would ensure good control loop stability margins, while the latter was used to furnish good airplane responses to turbulence and wind shear in terms of low rms and peak airspeed variations, rms elevator activity, and rms normal acceleration for good ride qualities.

The model used for the state estimator design is shown in Fig. 13. The feedback integrator, the ideal command response model, and the high-pass filter used in the LQR design (see Fig. 5) were not included in this model. The associated states are available directly and need not be included in the state estimator. It can be easily demonstrated that as long as their contributions to the control input are accounted for in the formulation of the LQG compensator, the separation theorem is still valid when they are combined with the state estimator.

The process noise and sensor noise intensities used are shown in Table 5. These were set as a compromise between robustness and airplane response to turbulence and wind shear. A key tradeoff in the design was the rms elevator activity in turbulence vs peak airspeed deviations in wind shear. For the ideal case of full-state feedback, the combination of low horizontal gust gain and high wind shear gain allow low elevator activity in turbulence combined with small peak airspeed deviations in wind shear. The performance obtained with the full-state design as shown in Fig. 14 cannot be obtained with a LQG compensator. The figure shows the tradeoff of turbulence vs wind shear performance for several state estimator designs with the estimated mean airspeed error $\Delta\hat{V}_m$ replacing ΔV_m in the construction of the feedback variable n_{zu}. For these designs, all process noise intensities were held fixed at the values in Table 5, except that the wind shear noise parameter s_n was allowed to vary as shown.

The LQG control law does not have wind shear rate information to feed back directly to the elevator. It uses instead a wind shear estimate based on filtered sensor data. The airspeed sensor measures both mean wind and turbulence. The estimator combines the airspeed and longitudinal acceleration to produce estimates of wind shear and turbulence velocities. Relatively small values of the noise intensity s_n produces a slow wind shear estimate. The result is that the airspeed is heavily filtered and elevator activity in turbulence is thus attenuated. The elevator response in wind shear is slow resulting in large speed deviations. Conversely, relatively large values of s_n produce a fast wind shear estimate and good control in wind shears. However, this results in increased elevator activity in turbulence. The method employed allows a straightforward tradeoff of elevator activity vs performance in wind shear. The selected design shown in Fig. 14 was based on the maximum acceptable level of elevator activity in turbulence. The wind shear design trades did not affect maneuver performance. The airspeed time history (unpiloted) due to a step shear input for the closed-loop airplane is shown in Fig. 15

Table 5 Noise spectral densities for estimator design

Process noise		Sensor noise	
U_n	1 $(ft/s)^2s$	V_{tn}	8×10^{-4} $(ft/s)^2s$
W_n	1 $(ft/s)^2s$	N_{zn}	2×10^{-7} $(g)^2s$
S_n	10^{-3} $(ft/s^2)s$	Q_n	4×10^{-6} $(deg/s)^2s$
D_{ecn}	10^{-3} $(deg/s)^2s$	H_n	5×10^{-5} $(ft/s)^2s$
V_n	1 $(ft/s^2)^2s$	$\dot{U}_n$	2×10^{-5} $(ft/s)^2$

Table 6 Stability margins and closed-loop roots

Flight condition	Cruise		V_{min}		V_{FC}/M_{FC}		Landing	
c.g.	18%	50%	18%	50%	18%	50%	18%	50%
Gain margin, dB	+27	+27	+27	+27	+30	+30	+27	+27
Phase margin, deg	80	58	68	61	120	51	73	70
Phugoid roots								
ζ	0.79	0.75	0.75	0.72	0.68	0.71	0.75	0.70
ω, rad/s	0.065	0.062	0.069	0.066	0.132	0.134	0.172	0.173
Short period roots								
ζ	0.57	0.65	0.72	0.65	0.57	0.51	0.83	0.92
ω, rad/s	3.02	1.57	2.01	1.09	3.18	1.40	2.02	1.68

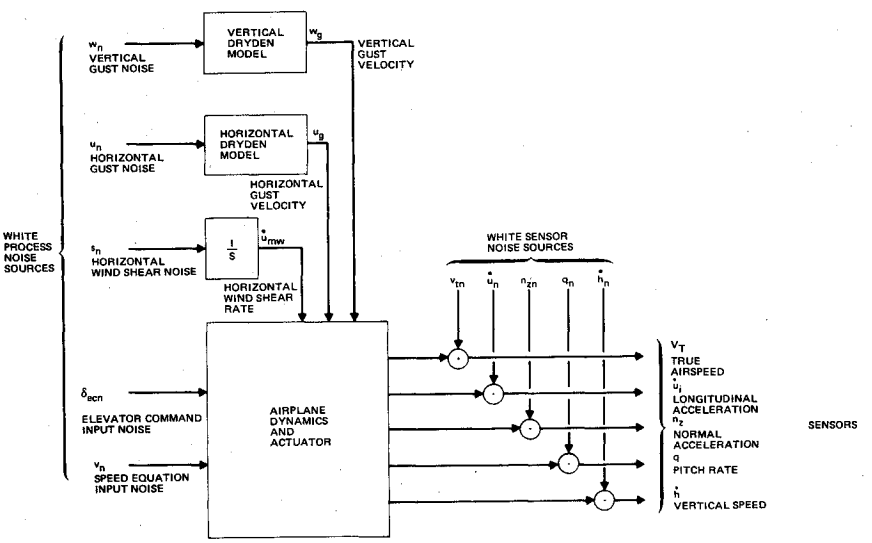

Fig. 13 State estimator synthesis model.

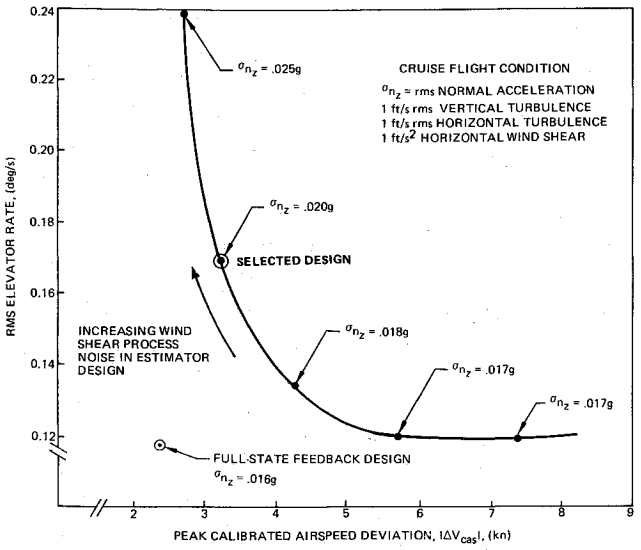

Fig. 14 RMS elevator rate due to horizontal and vertical turbulence vs peak air speed deviation in horizontal wind shear (rms normal acceleration values are also shown).

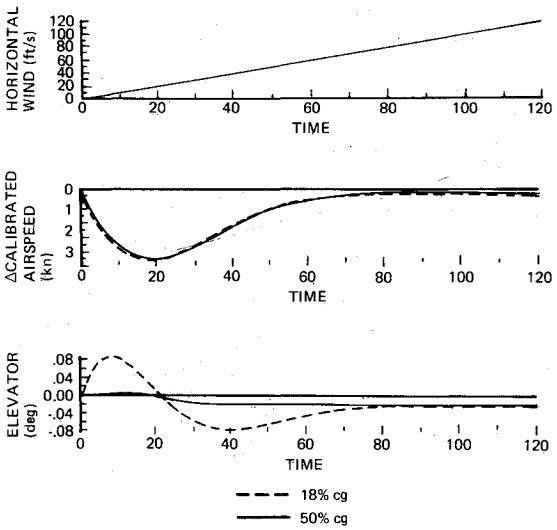

Fig. 15 Augmented airplane response to ramp tail wind shear, cruise flight condition: ---, 18% c.g.;—, 50% c.g.

and illustrates that the aircraft will return to its trim speed following a wind sheer input.

Elevator input noise δ_{ecn} was used to recover the full-state feedback stability margins at the input to the elevator actuator. In this way, the robustness characteristic of the full-state design was recovered. Analysis of the system at the low-speed flight condition revealed light damping of the speed estimate poles, due to a significant increase in the airplane phugoid frequency at low speeds. Additional noise was introduced into the speed equation to improve the robustness of the estimate of the mean airspeed.

The design resulted in a tenth-order state estimator that was reduced to eighth order by residualizing the highest bandwidth complex mode. This reduced-order estimator was combined with the feedback integrator and second-order loop gain low-pass filter to produce an eleventh-order feedback controller. The structure of the resulting closed-loop system is shown in Fig. 16. The elevator loop gain was scheduled as a function of dynamic pressure and flap position.

Control Performance

Response of the augmented airplane to column force commands are shown in Figs. 17-20. These responses compare with the responses of the unaugmented airplane (Figs. 1-4). There are significant improvements in the stability and response. These characteristics are relatively invariant with the flight condition and c.g. location.

The normalized pitch rate response to a column force step with speed fixed falls within the required envelope shown in Fig. 21 for one flight condition. Responses at other flight conditions also meet the criteria. The flying qualities criteria of Ref. 2 require that the short-period frequencies lie within bounds established as a function of the n_z/α coefficient. Figure 22 demonstrates that the criteria have been met for all flight conditions.

Elevator loop gain frequency responses are shown in Fig. 23. Stability margins and closed-loop eigenvalues are shown in Table 6. The high gain at low frequency, good loop gain crossover characteristics, and high-frequency attenuation are maintained at all flight conditions for all c.g. locations.

The control law was implemented on a motion base flight simulator. Extensive piloted tests were carried out by three test pilots who gave, for all c.g. locations and flight conditions, ratings equal to or better than those of the unaugmented airplane with excellent inherent stability and control characteristics. Particularly important characteristics were the

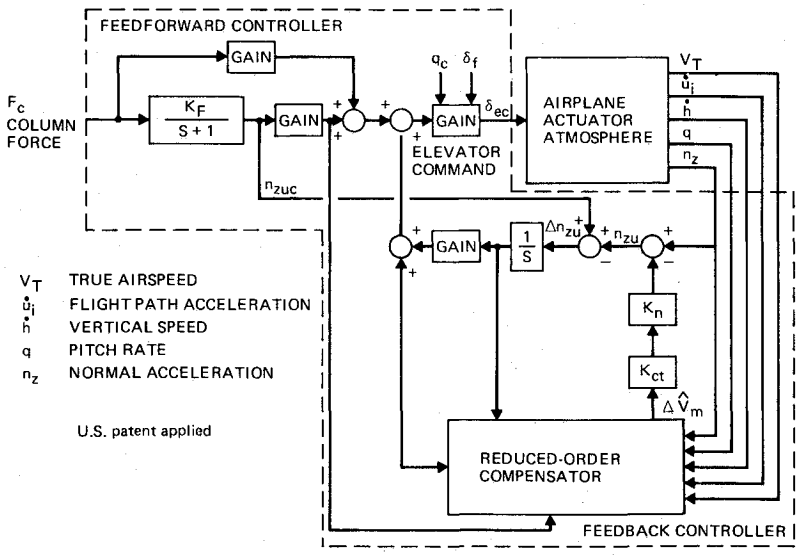

Fig. 16 Closed-loop system structure. Patent applied for.

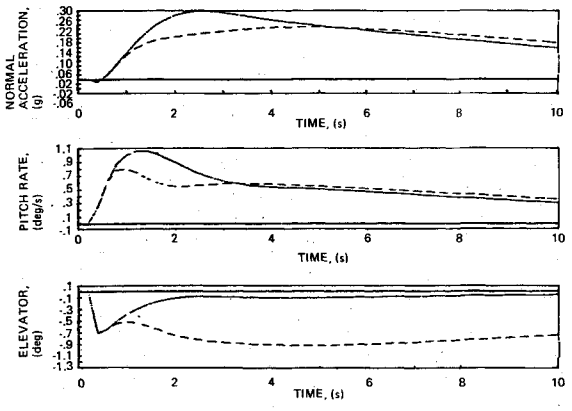

Fig. 17 Closed-loop short-period response at cruise flight condition.

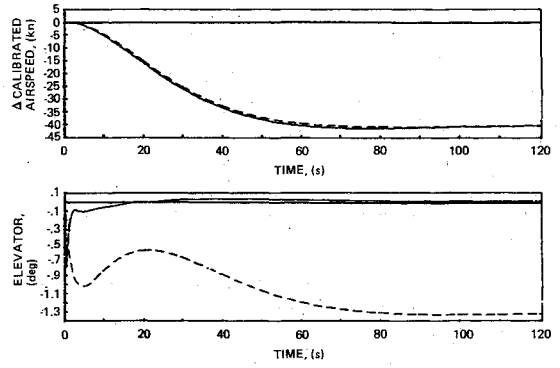

Fig. 18 Closed-loop speed response at cruise flight condition.

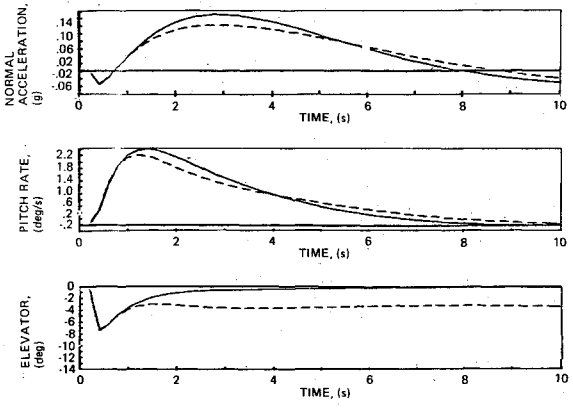

Fig. 19 Closed-loop short-period response at landing flight condition.

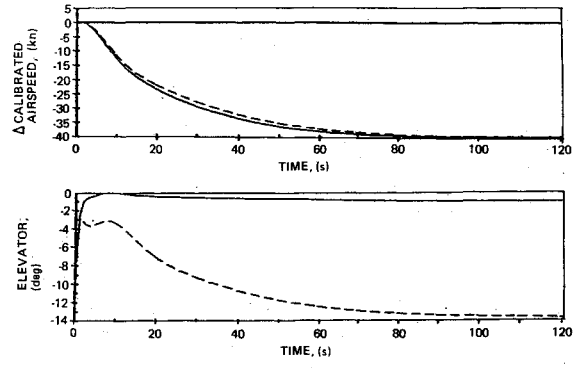

Fig. 20 Closed-loop speed response at landing flight condition.

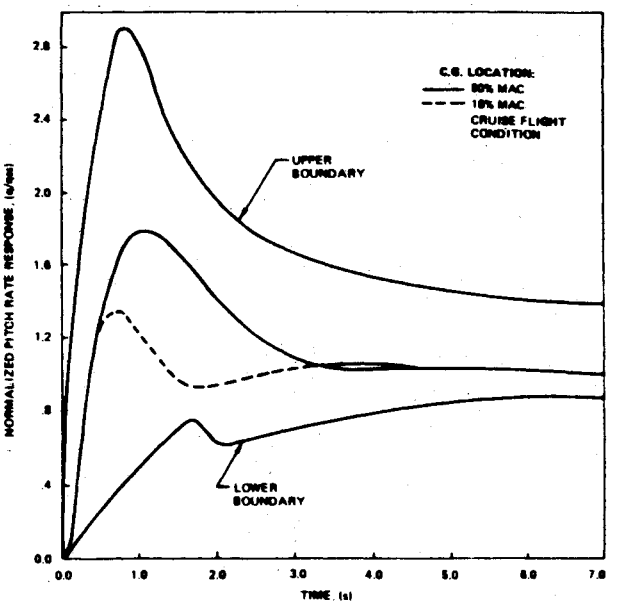

Fig. 21 Normalized pitch rate response.

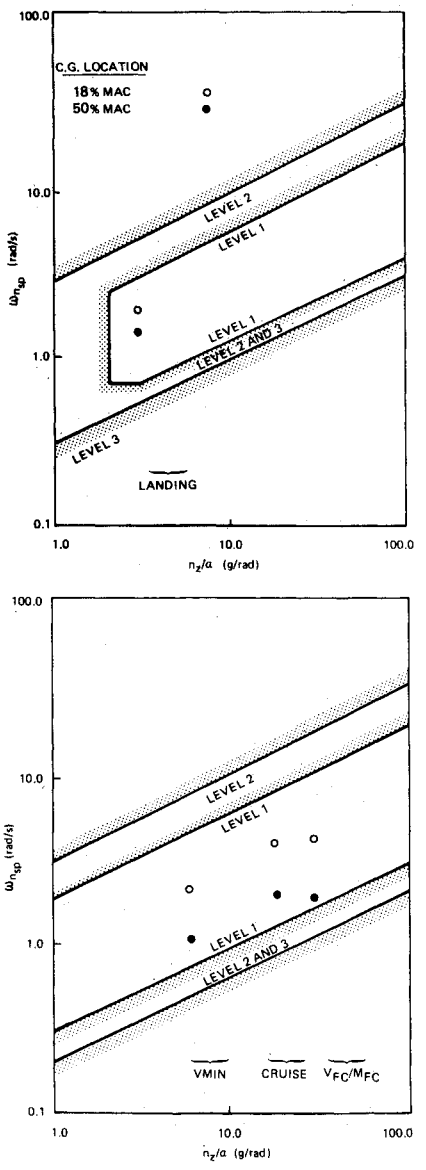

Fig. 22 Handling qualities based on short-period frequency.

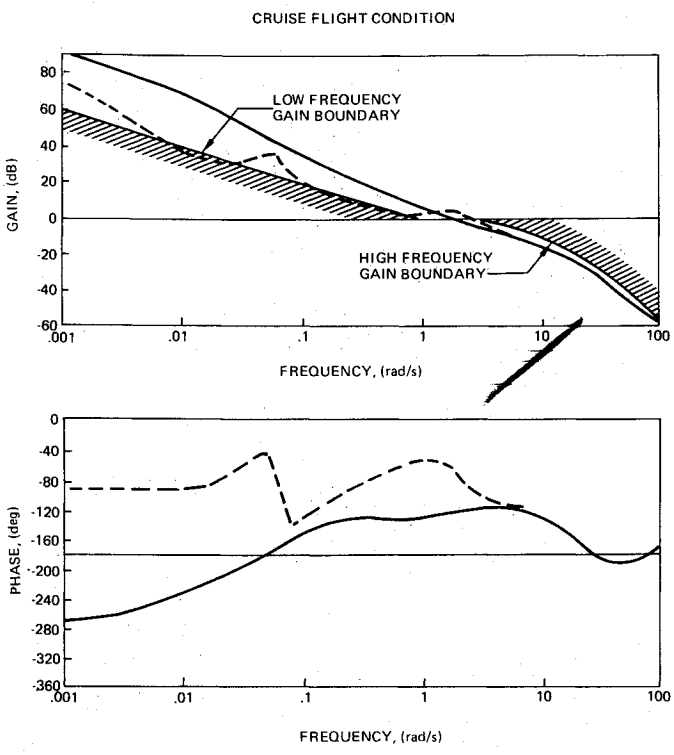

Fig. 23 Elevator loop gain Bode plot, cruise flight condition: ----, 18% cg; —, 50% cg.

task-tailored stick force gradients, the lack of phugoid oscillation, and the invariant handling qualities across the c.g. range and flight envelope.

Conclusions

The LQG control law design procedure allowed systematic implementation of the design requirements. The control law furnishes excellent handling qualities over the entire c.g. range and flight envelope. Airplane responses to pilot commands are similar for all configurations and flight conditions. The augmented aircraft exhibits normal angle-of-attack stability, thus furnishing standard speed stability characteristics. This is in contrast to concepts based on pitch attitude or flight path angle hold where the airplane trim is changed by momentary pilot inputs. Piloted simulations demonstrated that invariant stick force gradients will reduce the pilot workload and increase safety. Also, by furnishing an augmented airplane with "natural" response characteristics (i.e., similar to those of excellent unaugmented airplane), very little change in piloting technique will be required in the transition from today's airplanes to future airplanes with full-time command and stability augmentation.

Appendix: Synthesis Model Development

Begining with the standard rigid-body longitudinal state model having states u, α, q, and θ, actuator states and Dryden turbulence states[10] were added. The true airspeed V_T and mean airspeed V_m are defined as

$$V_T = u - u_{mw} - u_g \tag{A1}$$

Table A1 Flight condition: cruise with c.g. at 50% MAC

A matrix: states V_m, α, q, θ, δ_e, δ_{servo}, u_g, w_g, w_{g1}, u_{mw}

−0.01365	0.1780	0.00017	−0.5610	−0.03726	0.	0.01365	−0.01311	0.	−1.
−0.01516	−0.7520	1.001	0.00127	−0.06311	0.	0.01516	0.05536	0.	0.
0.00107	0.07896	−0.8725	0.	−3.399	0.	−0.00107	−0.00581	0.	0.
0.	0.	1.	0.	0.	0.	0.	0.	0.	0.
0.	0.	0.	0.	−20.00	10.72	0.	0.	0.	0.
0.	0.	0.	0.	0.	50.00	0.	0.	0.	0.
0.	0.	0.	0.	0.	0.	−0.4447	−0.0044	0.	0.
0.	0.	0.	0.	0.	0.	−0.0044	−0.4447	0.	0.
0.	0.	0.	0.	0.	0.	0.	0.	0.	0.

B matrix: inputs δ_{ec}, u_n, w_n, s_n, v_n

0.	0.	0.	0.	1.
0.	0.	0.	0.	0.
0.	0.	0.	0.	0.
0.	0.	0.	0.	0.
0.	0.	0.	0.	0.
50.00	0.	0.	0.	0.
0.	0.9431	0.	0.	0.
0.	0.	1.155	0.	0.
0.	0.	−48.82	0.	0.
0.	0.	0.	1.	0.

C matrix: outputs n_z, V_{cas}, $\dot{u}$, $\dot{h}$, q

0.00646	0.3203	−0.03358	0.	−0.1032	0.	−0.00646	−0.02358	0.	0.
0.3495	0.	−0.	0.	0.	0.	−0.3495	−0.	0.	0.
0.01365	0.1780	−0.00017	−0.5610	−0.03726	0.	−0.01365	−0.01311	0.	0.
0.	−13.58	0.	13.58	0.	0.	0.	0.	0.	0.
0.	0.	0.	0.	0.	0.	0.	0.	0.	0.

D matrix

0.	0.	0.	0.	0.
0.	0.	0.	0.	0.
0.	0.	0.	0.	0.
0.	0.	0.	0.	0.
0.	0.	0.	0.	0.

$$V_m = u - u_{mw} \tag{A2}$$

where u is the inertial speed, u_{mw} the mean horizontal wind velocity, and u_g the zero mean horizontal gust velocity. The mean wind term is modeled by

$$\dot{u}_{mw} = u_{mw} \tag{A3}$$

$$\dot{u}_{mr} = s_n \tag{A4}$$

where u_{mr} represents the mean wind rate and s_n is a zero-mean wind shear "noise" term used in the Kalman filter synthesis to adjust the convergence rate of the wind shear estimate. V_m replaced u as a state in the synthesis model through a similarity transformation. u_{mr} was removed from the resulting state equations to give a minimal realization. The resulting synthesis model is shown in Table A1.

The high-pass filter used for creating high-frequency attention in the control loop has the following state equations:

$$\begin{bmatrix} \dot{x}_1 \\ \dot{x}_2 \end{bmatrix} = \begin{bmatrix} 0 & 1 \\ -10{,}000 & -140 \end{bmatrix} \begin{bmatrix} x_1 \\ x_2 \end{bmatrix} + \begin{bmatrix} 0 \\ 1 \end{bmatrix} \delta_{ec}$$

$$y_u = \begin{bmatrix} -10{,}000 & -140 \end{bmatrix} \begin{bmatrix} x_1 \\ x_2 \end{bmatrix} + \delta_{ec} \tag{A5}$$

References

[1] "Integrated Application of Active Controls (IAAC) Technology to an Advanced Subsonic Transport Project – Initial ACT Configuration Design Study," NASA CR-159249, July 1980.

[2] Military Specification, "Flying Qualities of Piloted Airplanes," MIL-F-8785C, Nov. 1980.

[3] FAR 25, Federal Aviation Administration, 1978.

[4] Kwakernaak, H., and Sivan, R., *Linear Optimal Control Systems,* Wiley-Interscience, New York, 1972.

[5] Doyle, J.C., and Stein, G., "Multivariable Feedback Design: Concepts for a Classical/Modern Synthesis," *IEEE Transactions on Automatic Control,* Feb. 1981.

[6] Doyle, J.C. and Stein, G., "Robustness with Observers," *IEEE Transactions on Automatic Control,* Vol. AC-24, Aug. 1979, pp. 607-611.

[7] Gangsaas, D., Ly, U., and Norman, D.C., "Practical Gust Load Alleviation and Flutter Suppression Control Laws Based on LQG Methodology," AIAA Paper 81-0021, Jan. 1981.

[8] Lehtomaki, N.A., Sandell, N.R. Jr., and M. Athans, "Robustness Results in Linear Quadratic Gaussian Based Multivariable Control Design," *IEEE Transactions on Automatic Control,* Vol. AC-26, No. 1, Feb. 1981, pp. 75-92.

[9] Gupta, N.K., "Frequency-Shaped Cost Functionals: Extension of Linear-Quadratic-Gaussian Design Methods," *Journal of Guidance and Control,* Vol. 3, Nov.-Dec. 1980, pp. 529-535.

[10] Barr, N.M., Gangsaas, D., and Schaeffer, D.R., "Wind Models for Flight Simulator Certification of Landing and Approach Guidance Control Systems," FAA RD-74-206, Dec. 1974.

[11] Roskam, J., *Airplane Flight Dynamics and Automatic Flight Controls,* Roskam Aviation and Engineering Corporation, Ottawa, Kansas, 1979.